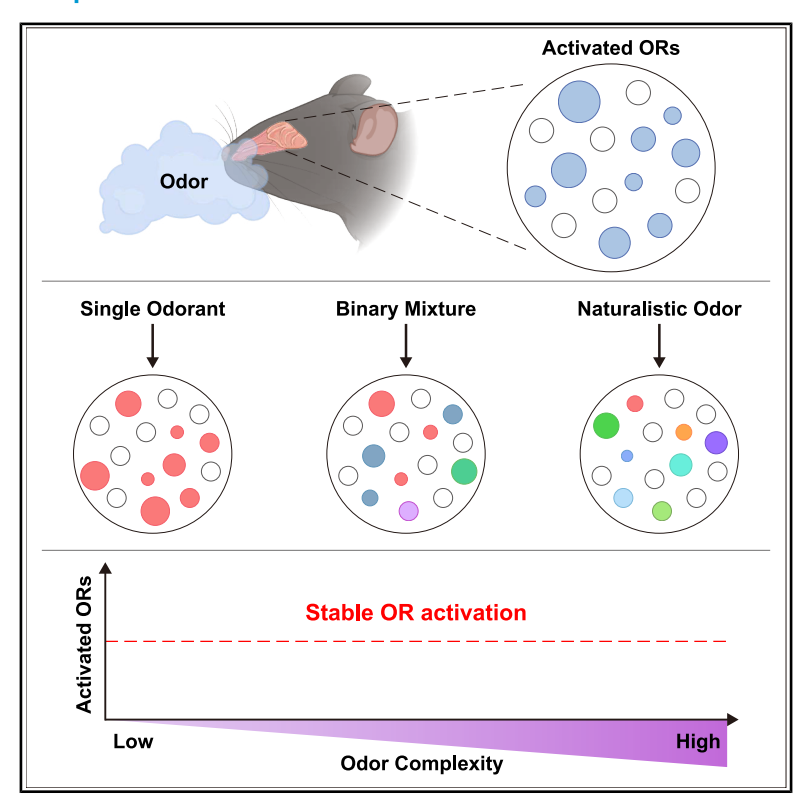
## **iScience**

# Stable olfactory receptor activation across odor complexity

#### **Graphical abstract**



#### **Authors**

Minseok Kim, Jeongyoon Lee, Inah Park, ..., Hyuk-Jun Kwon, Cheil Moon, Han Kyoung Choe

### Correspondence

choehank@dgist.ac.kr

#### In brief

Natural sciences; Biological sciences; Neuroscience; Sensory neuroscience

### **Highlights**

- Most odor mixtures induce OR activation patterns close to the linear sum of components
- A subset of ORs shows non-linear responses, including suppression and mixture-specific activation
- The number of activated ORs remains stable despite increasing odor complexity
- PhosphoTRAP enables global profiling of OR responses across odor complexities





## **iScience**



#### **Article**

# Stable olfactory receptor activation across odor complexity

Minseok Kim,<sup>1,2</sup> Jeongyoon Lee,<sup>3</sup> Inah Park,<sup>2</sup> Jihoon Kim,<sup>2</sup> Keunsoon Lee,<sup>5</sup> Jinhyun So,<sup>4</sup> Ji-Woong Choi,<sup>4</sup> Jae Eun Jang,<sup>4</sup> Hyuk-Jun Kwon,<sup>2,4</sup> Cheil Moon,<sup>1,2</sup> and Han Kyoung Choe<sup>1,2,3,6,\*</sup>

<sup>1</sup>Department of Brain Sciences, Daegu Gyeongbuk Institute of Science and Technology, 333 Techno Jungang-daero, Hyeonpung-eup, Dalseong-gun, Daegu 42988, Republic of Korea

<sup>2</sup>Convergence Research Advanced Centre for Olfaction, Daegu Gyeongbuk Institute of Science and Technology, 333 Techno Jungang-daero, Hyeonpung-eup, Dalseong-gun, Daegu 42988, Republic of Korea

<sup>3</sup>Brain Sciences Research Center, Daegu Gyeongbuk Institute of Science and Technology, 333 Techno Jungang-daero, Hyeonpung-eup, Dalseong-gun, Daegu 42988, Republic of Korea

<sup>4</sup>Department of Electrical Engineering and Computer Science, Daegu Gyeongbuk Institute of Science and Technology, 333 Techno Jungang-daero, Hyeonpung-eup, Dalseong-gun, Daegu 42988, Republic of Korea

<sup>5</sup>R&D Unit, ScentOn, 306 Teheran-ro, Gangnam-gu, Seoul 06210, Republic of Korea

<sup>6</sup>Lead contact

\*Correspondence: choehank@dgist.ac.kr https://doi.org/10.1016/j.isci.2025.113740

#### **SUMMARY**

Mechanisms underlying single odorant activation of specific olfactory receptors are well understood. However, how the olfactory system processes complex odor mixtures at the receptor level remains unclear. This study examined olfactory receptor activation patterns across odor complexities using phosphoTRAP analysis. For most mixtures, receptor activation patterns closely matched the linear sum of individual component responses. However, distinct receptor sets display non-linear responses unexplained by linear models. Mixture responses were generally located between component responses and often aligned with linear predictions, though some deviations indicated non-linear interactions. Total activated receptors remained relatively constant regardless of odor complexity, suggesting efficient coding that prevented receptor saturation as odorant components increased. These findings provide receptor-level evidence that the olfactory system encodes complex odors primarily through linear integration of receptor activity, with added specificity from non-linear responses in limited receptors, advancing understanding of how the olfactory system normalizes receptor activation in response to natural odors.

#### INTRODUCTION

The mammalian olfactory system has a remarkable ability to detect and discriminate an immense diversity of odors, a function essential for survival, behavior, and social interactions. <sup>1,2</sup> This extraordinary sensitivity is achieved through the expression of a large repertoire of olfactory receptor (OR) genes, each typically expressed in a single olfactory sensory neuron (OSN). <sup>3,4</sup> Through a combinatorial coding strategy, each odorant can activate multiple ORs, and each OR can respond to multiple odorants, enabling the system to represent a vast array of odor identities with a finite receptor repertoire. <sup>5,6</sup>

Over the past decades, elucidation of how individual odorant molecules interact with their binding receptors, including atomic-level insights from structural studies and large-scale mapping of odorant-receptor pairs, has advanced. Tell Sequencing-based approaches have revealed that even a single odorant often recruits a characteristic and sometimes a broad subset of ORs, reflecting the diversity of tuning breadths among receptors.

these studies have focused on responses to single odorants or simple binary mixtures, which do not capture the complexity of natural olfactory stimuli. <sup>15,16</sup> In natural environments, most odors are complex mixtures containing dozens to hundreds of volatile compounds. <sup>17</sup>

Processing such complex mixtures presents a fundamental challenge for the olfactory system. Behavioral and physiological studies have shown that as mixture complexity increases, identifying individual components becomes more challenging for animals and humans, and mixtures are often perceived as unique odor objects rather than the sum of their parts. <sup>18,19</sup> At the cellular level, studies using calcium imaging, dissociated OSNs, and *in vitro* assays have demonstrated that responses to binary mixtures can exhibit both linear summation and pronounced non-linear interactions, such as suppression or emergent activation. <sup>16,20–23</sup> However, how these principles extend to the full receptor repertoire when challenged with the complexity of naturalistic odors remains unclear. In particular, whether increasing odor complexity leads to a proportional increase in the number of activated ORs, which could risk saturating the coding capacity





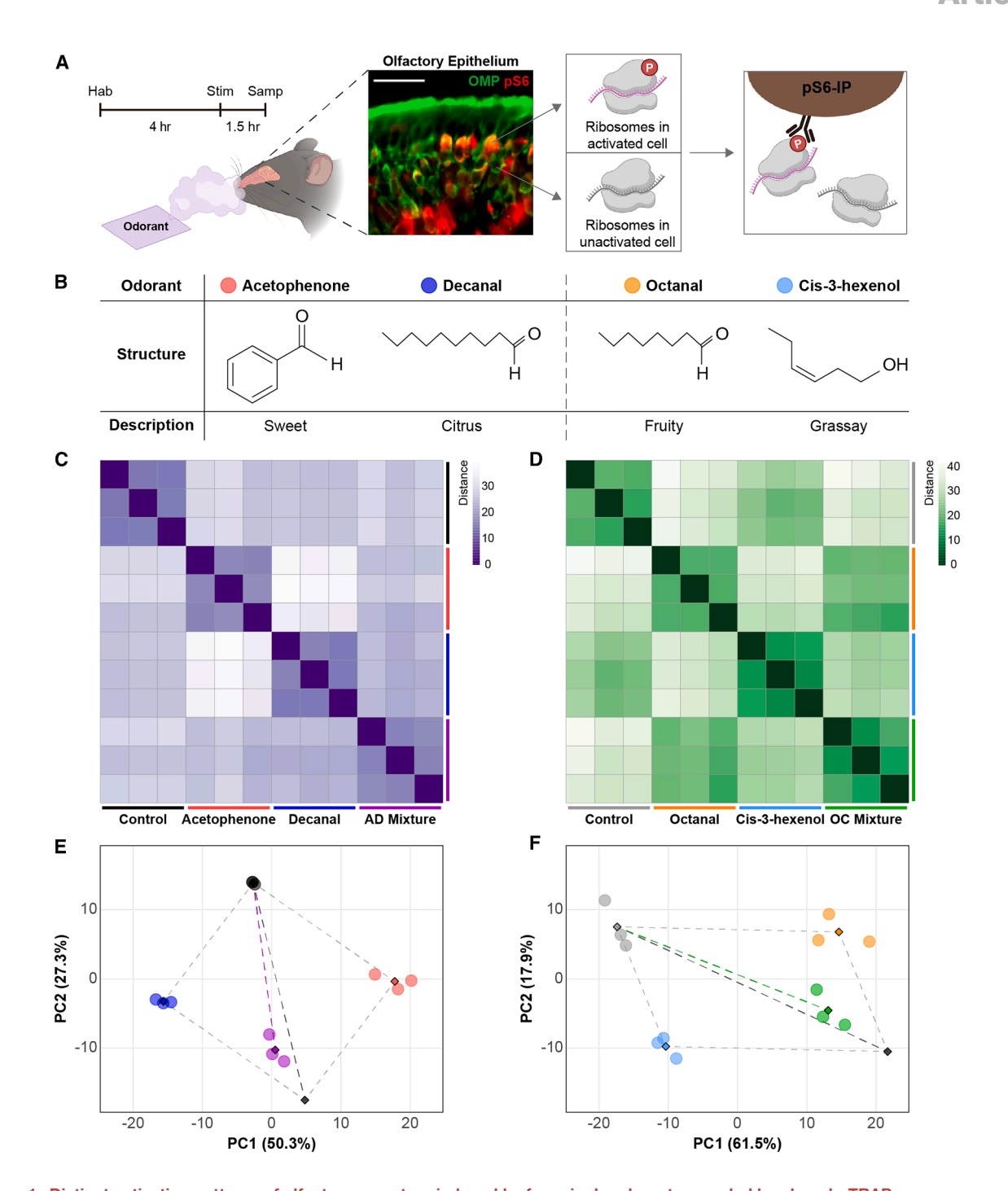


Figure 1. Distinct activation patterns of olfactory receptors induced by four single odorants revealed by phosphoTRAP

(A) Schematic diagram of the experimental workflow. Mice were habituated for 4 h (Hab), exposed to a single odorant for 1.5 h (Stim), and the olfactory epithelium (OE) was sampled (Samp). Immunostaining of OE shows olfactory marker protein (OMP, green) and phosphorylated S6 ribosomal protein (pS6, red) in activated

cells. Only ribosomes in activated cells are phosphorylated and selectively captured by pS6 immunoprecipitation (pS6-IP). Scale bars, 10 µm (B) Chemical structures and descriptions of the four odorants used for stimulation: acetophenone (red, sweet), decanal (blue, citrus), octanal (orange, fruity), and cis-3-hexenol (sky blue, grassy).

(C and D) Distance matrices presenting the similarity in OR activation patterns for acetophenone, decanal, and their mixture (AD) (C), and for octanal, cis-3-hexenol, and their mixture (OC) (D). Each row and column represents an individual sample.

(legend continued on next page)



of the system, or whether mechanisms exist to constrain receptor recruitment and maintain efficient coding, is unclear. 15,24,25

Therefore, this study aimed to systematically examine OR activation patterns in response to a spectrum of odor complexities, ranging from single odorants to binary mixtures and complex naturalistic fragrances. Our study provides insight into how the olfactory system maintains both efficiency and discriminative power in the face of natural odor complexity.

#### **RESULTS**

## Molecular profiling of odor-evoked OR activation using phosphoTRAP

First, we assessed the odor investigation behavior. Mice were alternately exposed for 5 min to empty filter paper (no odor, control) and odor-applied filter paper. In each experiment, mice were exposed to three odorants per experiment, and over three days, all nine odorants were tested. The order of odorant exposure was randomized to avoid sequence bias (n=7; Figures S1A and S1B). The number of odor investigations did not differ significantly across odor conditions, and the distance traveled within the cage during each session was similar (Figures S1C and S1D). The location of the mice during each odor session was recorded as heatmaps (Figures S1E–S1O). Thus, mice exhibited neither innate preference nor aversion to any of the odorants tested.

Upon binding of an odorant molecule, the OR activates the G protein Golf, which subsequently stimulates adenylyl cyclase III (ACIII). 26,27 ACIII catalyzes ATP conversion to cyclic AMP (cAMP), raising intracellular cAMP levels and opening cyclic nucleotide-gated ion channels.<sup>3,28</sup> The resulting influx of Na<sup>+</sup> and Ca<sup>2+</sup> ions leads to neuronal depolarization and activation of the mTORC1 pathway, ultimately activating S6 kinase and resulting in the phosphorylation of ribosomal protein S6 in the stimulated OSNs (Figure S2A). 29,30 Phosphorylation of S6 protein, thereby, serves as a useful marker to survey neural activation.<sup>31</sup> To examine the activation profile of phosphorylated ribosomal protein S6 (pS6) in OSN in vivo, we performed immunohistochemical analysis on olfactory epithelium (OE) sections obtained from mice exposed either to a no-odor control or to 100% acetophenone. In odor-exposed OE sections, pS6 expression within mature OSNs increased, as identified by co-labeling with olfactory marker protein (Figures S2B and S2C). In contrast, pS6 levels in OSNs from control animals remained at baseline levels. These results support previous findings indicating that odorant exposure increases pS6 phosphorylation in mature OSNs within the OE.14 Activity-dependent pS6 acts as a sensitive molecular marker of recent neuronal activation and is the molecular substrate for ribosome capture in the phosphoTRAP assay. 32

To further verify odor-evoked activation in the OE, western blot analyses of OE tissue were performed after exposure to each odor condition. Immunoblotting for pS6 and  $\beta$ -actin revealed

increased pS6 signal in samples from odor-exposed mice compared to controls. This result provided additional molecular evidence that odor stimulation robustly induced pS6 expression in the OE (Figures S2D and S2E).

We used phosphoTRAP (Figure 1A) to investigate the activation patterns of ORs in response to odor stimuli. This method enables molecular profiling of activated ORs by capturing the phosphorylation of pS6, a neuronal activation marker. Because each OSN expresses only one type of OR, this approach allows for precise mapping of receptor activation.<sup>33</sup> Mice were exposed for 90 min to four distinct odorants (100% concentration of acetophenone [A], decanal [D], octanal [O], and *cis-3*-hexenol [C]) or their binary mixtures (acetophenone and decanal [AD] and octanal and *cis-3*-hexenol [OC]) applied onto a filter paper, with empty filter paper serving as a no-odor control (Figures 1A and 1B). Following exposure, total RNA and pS6-associated mRNA were analyzed using next-generation sequencing.

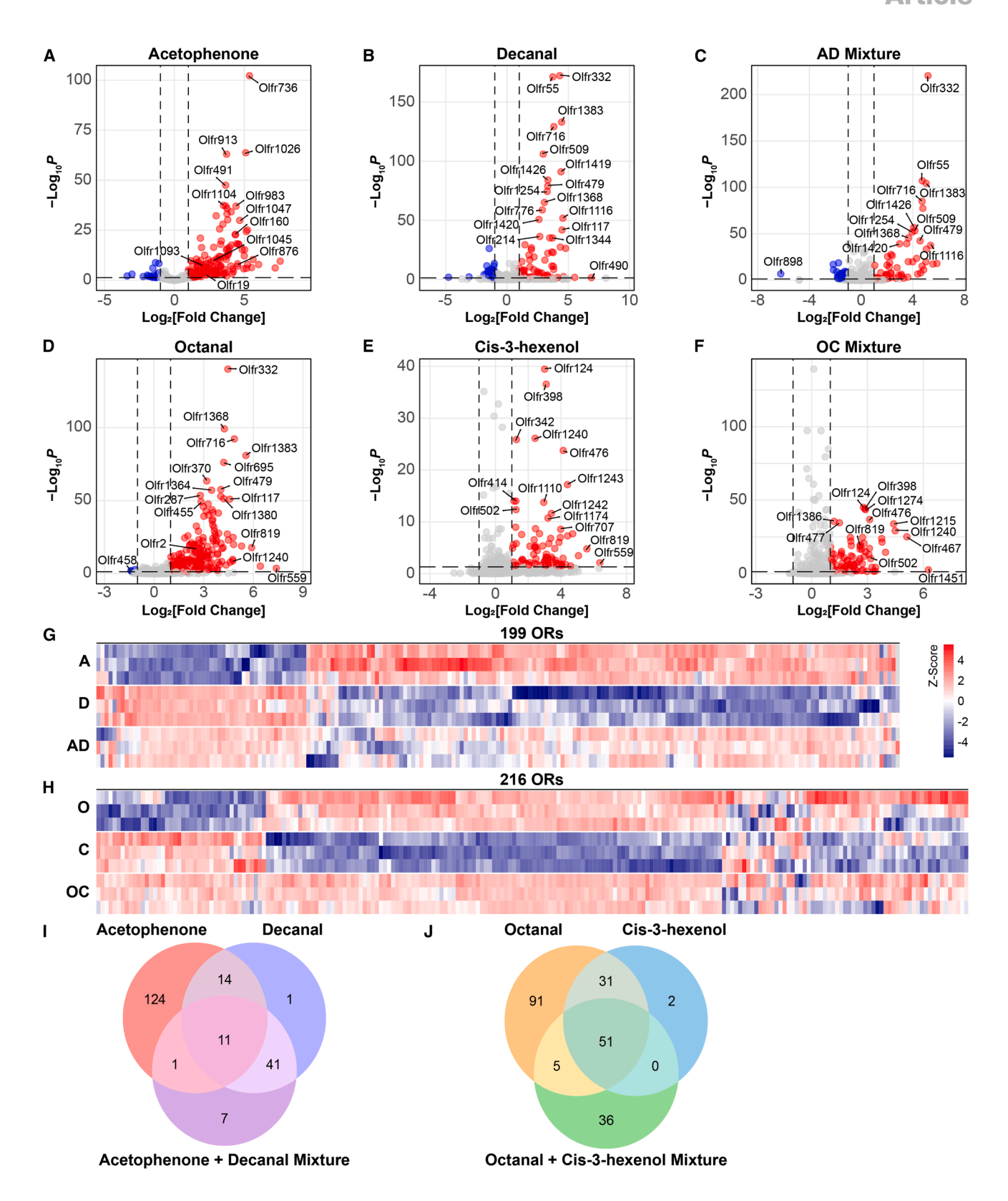
Sequencing data analysis revealed distinct enrichment patterns between total RNA and phosphoTRAP samples in response to each odor stimulus. Distance matrices of these datasets showed darker colors along the diagonal, indicating strong similarity among replicates exposed to the same condition, which supports the reliability of our approach (Figures S3A and S3B). When comparing the clustering ability of both approaches, principal-component analysis (PCA) of total RNA failed to effectively separate individual odorant conditions (Figures S3C and S3D), whereas that of phosphoTRAP samples demonstrated clearer segregation of odorant conditions, reflecting the enhanced specificity of this approach for capturing neuronal activation (Figures S3E and S3F).

To further understand the activation patterns of ORs, we focused on OR-encoding transcripts enriched in phosphoTRAP samples. Correlation analysis of these OR activation patterns showed high reproducibility among replicates for each odorant stimulus (Figures 1C and 1D) (see also Data S1A and S1B for log2 fold changes and p values of ORs). Distinctive response patterns were observed among individual odorants. While odorant mixtures were not identical to their single components, they exhibited partial similarity to both. In both odorant sets, PCA analysis clearly showed that the OR activation pattern of the mixture was distinct yet intermediate, with the cluster representing the odorant mixture located between the clusters of its constituent single chemicals (Figures 1E and 1F). For example, in the A, D, and AD conditions, the AD mixture cluster was positioned between A and D. In the O, C, and OC conditions, the OC cluster was found between O and C, albeit closer to O than C. Although cluster positions of mixed odorants were in the direction of the vector sum of their individual odorant clusters, the magnitude was less than that of the summed vector.

Similarly, the analysis of the full OR activation space demonstrated high correlation of the predicted response to mixtures (as a linear combination of individual odorant responses) with

(E and F) Principal-component analysis (PCA) plots of OR activation patterns for each odor pair and their mixtures; (E) acetophenone (red), decanal (blue), AD mixture (purple), and control (black) groups are shown; (F) octanal (orange), *cis*-3-hexenol (sky blue), OC mixture (green), and control (gray) groups are shown. Each circle indicates an individual mouse (*n* = 3 per group), while colored diamonds represent group means. Dashed lines indicate vectors from control to each condition, and black diamonds represent the vector sum of single odorant responses. The percentage of variance explained by each principal component is indicated on the axes (PC1 and PC2).





(legend on next page)



the actual measured response (Figures S3G and S3H). The overall response characteristics of ORs suggested that the response patterns to mixed odorants closely resembled the sum of their individual components. Nonetheless, some discrepancies between observed OR activation patterns and simple linear summation implied that the responses to mixture involved nonlinear mechanisms in a minority of ORs. Thus, the abundance of OR genes detected by phosphoTRAP analysis provides a robust molecular readout of the OE's response to odorant stimulation.

## Binary odorant mixtures induce complex OR activation patterns encompassing linear and non-linear interaction

To address how each OR responds to single odorants and their binary mixtures, we analyzed the differential expression patterns of individual ORs in phosphoTRAP data. Volcano plot analysis revealed distinct OR activation signatures for each condition (Figures 2A–2F). Significantly upregulated ORs (fold change  $\geq$  2, p value  $\leq$  0.05) were identified across all test conditions: 150 ORs for A (Figure 2A), 67 for D (Figure 2B), 178 for O (Figure 2D), and 84 for C (Figure 2E). We also detected significantly upregulated ORs in binary mixtures: 60 ORs responding to the AD mixture (Figure 2C) and 92 to the OC mixture (Figure 2F) (see also Data S2A and S2B for lists of significantly upregulated ORs).

Although we also observed a minor population of downregulated ORs, the suppression of OR responses could play an important role in combinatorial coding and non-linear mixture effects, and future investigations will be necessary to elucidate their biological contributions (see also Data S3A and S3B for lists of significantly downregulated ORs).

To further compare individual odorant and binary mixture-evoked receptor activation, we generated heatmaps of ORs that exhibited statistically significant or above-threshold fold changes in at least one condition. For visualization, expression values were transformed to Z score to emphasize relative differences across conditions. This analysis revealed that ORs activated by A displayed distinct profiles from those responding to D. Notably, most receptors responsive to either A or D also responded to their mixture (AD), whereas a subset of ORs that were activated by single odorants failed to respond in the mixture. A similar pattern was observed for O, C, and their mixture (OC) (Figures 2G and 2H).

Venn diagram analysis revealed intricate patterns of OR activation in response to binary mixtures (Figures 2I and 2J). For the A and D combination (Figure 2I), most OR responses were specific

to one component or the mixture itself. In total, 124 ORs responded exclusively to A, whereas only one OR responded exclusively to D. An overlap of one OR was observed between A and the AD mixture, whereas a larger overlap of 41 ORs occurred between D and the AD mixture. Notably, 11 ORs were upregulated across all three conditions, demonstrating consistent activation regardless of stimulus complexity. In addition, two distinct populations of non-linear mixture-responsive ORs were identified. One group comprised 14 ORs that responded to both single odorants but showed no response to the mixture, suggesting inhibitory interactions when these odorants are combined. The second group comprised seven mixture-specific ORs that were not activated by either single odorant, indicating emergent activation patterns unique to the AD mixture.

For the O and C combination (Figure 2J), we observed similar complexity but with different proportions. In total, 91 ORs responded exclusively to O, whereas only two ORs responded exclusively to C. A total of 51 ORs were upregulated across all three conditions, showing a higher degree of overlap compared to the AD mixture. Additionally, 31 ORs that responded to single odorants showed no response to the OC mixture, further supporting inhibitory mechanisms in this context. Notably, 36 mixture-specific ORs were identified that were not activated by either single odorant. This represents a substantial proportion of emergent responses unique to the OC mixture (see also Data S2 and S3 for lists of significantly up- or downregulated ORs).

These findings show that binary odorant mixtures activate most receptors that respond to one of the component odorants. In addition, non-linear emergent activation produces response patterns to the mixture that differ from simple linear combinations of individual odorant responses. This suggests that complex integration mechanisms are at work at the receptor level.

To address whether the method of binary odor mixture delivery influences OR activation, we established two experimental paradigms. In the "mixture" condition, both odorants were applied together onto a single piece of filter paper. In contrast, in the "separated" condition, each odorant was dispensed onto its own filter paper, with the two papers placed side by side approximately 1 mm apart, preventing potential direct liquid-phase interactions before volatilization (Figure S4A).

Following odor stimulation, phosphoTRAP analysis of the olfactory epithelial tissue was performed, and the enrichment of ORs was exclusively analyzed. PCA based on the OR activation profiles revealed no clear separation between samples exposed to the mixture condition (triangles) and those exposed to the separated condition (squares) (Figures S4B and S4C; see also Data S1C for log2 fold changes and p values for ORs). A

#### Figure 2. Comparative analysis of activated olfactory receptors in response to single odorants and binary mixtures

(A–F) Volcano plots showing differential expression of olfactory receptors (ORs) for each odorant condition: (A) acetophenone, (B) decanal, (C) AD mixture, (D) octanal, (E) cis-3-hexenol, and (F) OC mixture. Red dots indicate significantly upregulated ORs (fold change  $\geq$  2, p value  $\leq$  0.05), blue dots indicate significantly downregulated ORs (fold change  $\leq$  -2, p value  $\leq$  0.05), and gray dots represent ORs with non-significant changes.

(G and H) Heatmaps showing expression patterns of significantly regulated ORs across odor conditions. (G) Shows data for acetophenone (A), decanal (D), and AD mixture. (H) Shows data for octanal (O), *cis*-3-hexenol (C), and OC mixture. Expression levels were normalized by *Z* score transformation to emphasize relative up- or downregulation across conditions, with red and blue representing up- and downregulated expression, respectively.

(I and J) Venn diagrams summarizing the overlap of significantly upregulated ORs between individual odorants and their mixtures. (I) Acetophenone, decanal, and AD mixture. (J) Octanal, cis-3-hexenol, and OC mixture. The diagrams highlight the unique and shared receptor activations, illustrating both linear and non-linear mixture effects.



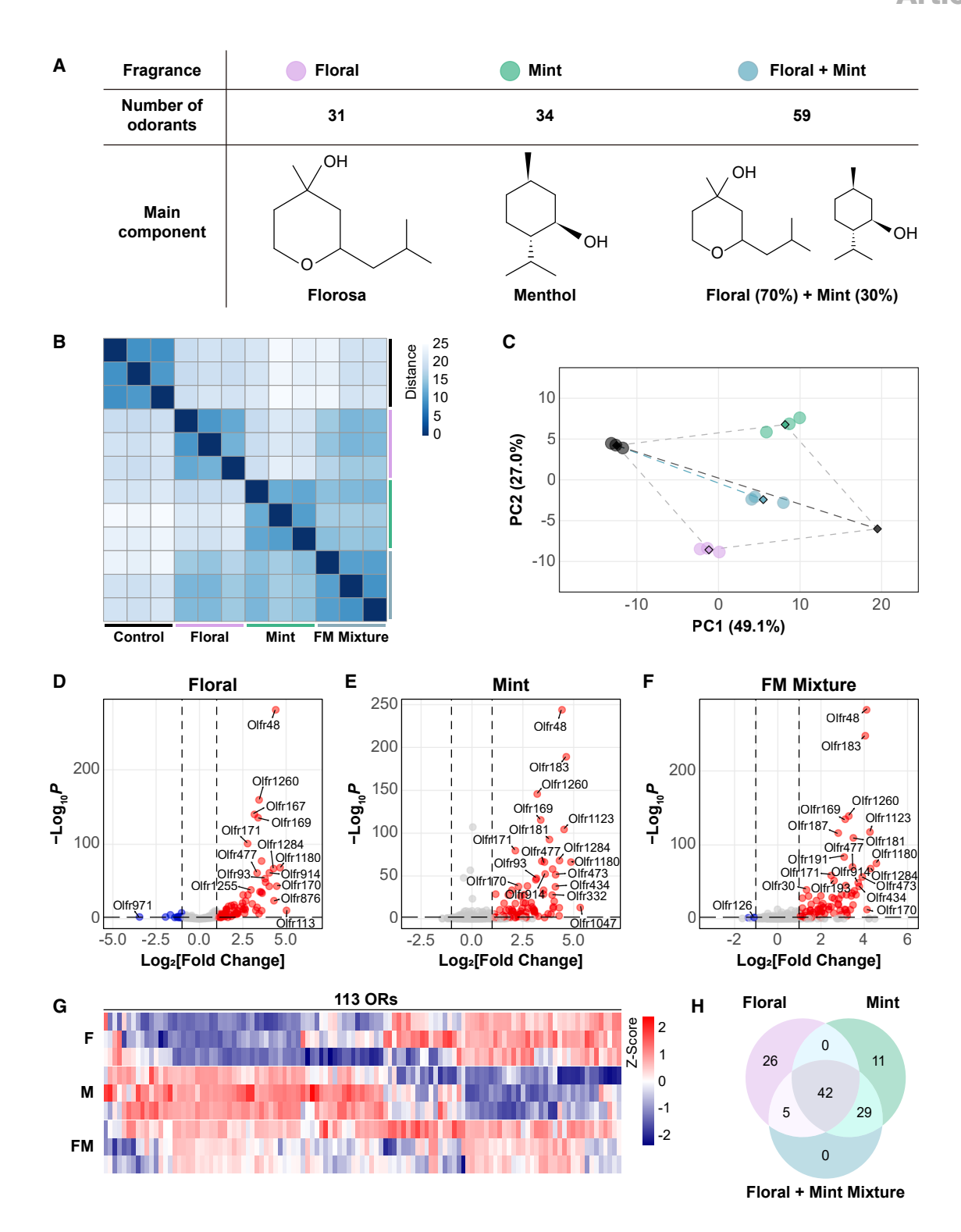


Figure 3. Olfactory receptor activation patterns in response to naturalistic fragrances and their mixture

(A) Naturalistic fragrances used for stimulation: floral (pink, 31 compounds including florosa), mint (teal, 34 compounds including menthol), and FM mixture (floral 70% + mint 30%, blue). The main components and descriptions of the fragrances are shown.

(B) Distance matrix depicting the similarity of olfactory receptor (OR) activation patterns across floral, mint, and FM mixture conditions. Samples are clustered based on pairwise distances of OR expression profiles.

(legend continued on next page)



comprehensive analysis of the OR activation spectrum in both conditions showed a very strong correlation between the mixture and separated groups (Figures S4D and S4E), indicating highly similar OR activation patterns regardless of the delivery method.

To explore the distribution of significantly upregulated ORs, we plotted Venn diagrams. In both odorant combinations tested, the majority of ORs activated in the separated condition also appeared among those activated in the mixture condition. Notably, the mixture group tended to recruit a small subset of ORs that were not observed in the separated group (Figures S4F and S4G) (see also Data S2C and S3C for lists of significantly upor downregulated ORs). Thus, direct chemical interactions occurring when odorants are physically mixed may contribute to an emergent OR activation.

## Naturalistic fragrances and their mixtures induce complex OR activation patterns encompassing linear and non-linear interaction

Natural odors typically comprise complex mixtures containing dozens to hundreds of volatile compounds. <sup>17</sup> To investigate whether the principles previously observed with single chemical odorants and their mixtures also apply to naturalistic fragrances, we studied the OR responses to commercially available perfumes constructed based on fragrance principles and their mixtures

We selected two distinctive complex fragrances: floral (F, containing 31 compounds, including florosa) and mint (M, containing 34 compounds, including menthol). Six chemicals were common constituents of these two fragrances. For mixture (FM), we blended floral and mint fragrance in a 7:3 ratio (Figure 3A).

Using phosphoTRAP analysis, we examined OR activation patterns in response to either F, M, or their mixture FM. Analysis of the sample distance matrix revealed that these conditions continued to induce distinct and separable OR activation patterns (Figure 3B). The analysis was restricted to OR-encoding genes within the phosphoTRAP data, and PCA revealed clear discrimination among the odor stimuli (Figure 3C). Consistent with the findings for single chemical odorants and their mixtures (Figures 1E and 1F), the OR activation pattern for FM was positioned between those for F and M. Notably, the distance of FM from the control was less than that of the summed vector of F and M.

Volcano plot analysis identified differentially expressed ORs (fold change  $\geq 2$ , p value  $\leq 0.05$ ) across all test conditions: 73 ORs for F fragrance (Figure 3D), 82 for M fragrance (Figure 3E), and 76 for the FM mixture (Figure 3F) (see also Data S1D for log2 fold changes and p values of ORs). Heatmap visualization of differentially expressed ORs also illustrated the linear and

non-linear relationship between individual fragrance and their mixture (Figure 3G). Venn diagram analysis revealed intricate patterns of OR recruitment in response to these complex fragrances (Figure 3H) (see also Data S2D and S3D for lists of significantly up- or downregulated ORs). Twenty-six ORs responded exclusively to F fragrances, while 11 ORs were specific to M fragrances. The FM showed partial overlap with both F and M fragrances; five ORs were shared between F and mixture, whereas 29 ORs were common between M and FM. In addition, 42 ORs were upregulated across all three conditions. No unique ORs were exclusively activated by the mixture. These results extend our findings from single odorants and binary mixtures to more naturalistic, complex fragrances.

Similar to our observations with binary mixtures, the FM mixture exhibited a non-linear activation pattern that was not simply the weighted sum of its components. This finding reinforces the idea that non-linear integration is a fundamental property of olfactory processing that extends from simple binary mixtures to complex naturalistic odors.

#### Activated OR count remains consistent despite increasing odor complexity

We observed both linear and non-linear OR responses to mixed odorant stimuli, prompting us to investigate how receptor activation scales with increasing odorant complexity. To address this, we first plotted the number of constituent chemicals in each odorant and complex odor experiment against the number of activated ORs (Figure 4A). The increasing number of chemical compounds in the odor stimulus did not lead to a corresponding increase in OR activation.

The experiments involving single chemical compounds and their mixtures differed significantly in the number of constituent chemicals compared to the experiments with naturalistic fragrances and their mixtures. Statistical comparisons using Kolmogorov-Smirnov tests confirmed no significant differences between any pairwise comparisons (single vs. binary: p = 0.9333; single vs. complex: p = 0.2286; binary vs. complex: p = 0.9000). This indicates that the olfactory system engages similar numbers of receptors regardless of odor complexity. We also counted the number of OR in single chemical compounds (single), binary compound mixture (binary), and naturalistic fragrances and their mixture (complex) (Figure 4B). One-way ANOVA comparing all three groups showed no significant differences in mean activated OR counts (p = 0.3188).

Based on these observations, we propose a model for olfactory coding characterized by linear and non-linear integration at the receptor level (Figure 4C). When odors are mixed, individual odorresponsive ORs remain active while others are suppressed, and

<sup>(</sup>C) Principal-component analysis (PCA) of OR activation patterns with samples colored as floral (pink), mint (teal), FM mixture (blue), and control (black). Circles represent individual mice (n = 3 per group), while colored diamonds indicate group means. Dashed lines represent vectors originating from the control condition to each odor condition, with the black diamond denoting the vector sum of floral and mint. The percentage of variance explained by each principal component is indicated on the axes (PC1 and PC2).

<sup>(</sup>D–F) Volcano plots illustrating differentially expressed ORs for floral (D), mint (E), and FM mixture (F) stimuli. Red dots mark significantly upregulated ORs (fold change  $\geq$  2, p value  $\leq$  0.05), blue dots denote significantly downregulated ORs (fold change  $\leq$  -2, p value  $\leq$  0.05), and gray dots correspond to non-significant changes.

<sup>(</sup>G) Heatmap showing expression patterns of 113 significantly regulated ORs across floral (F), mint (M), and FM mixture (FM) conditions. Data are normalized using Z score transformation, with red indicating higher expression and blue indicating lower expression relative to each OR's mean.

<sup>(</sup>H) Venn diagram summarizing the overlap and unique distribution of significantly upregulated ORs among floral, mint, and FM mixture conditions.



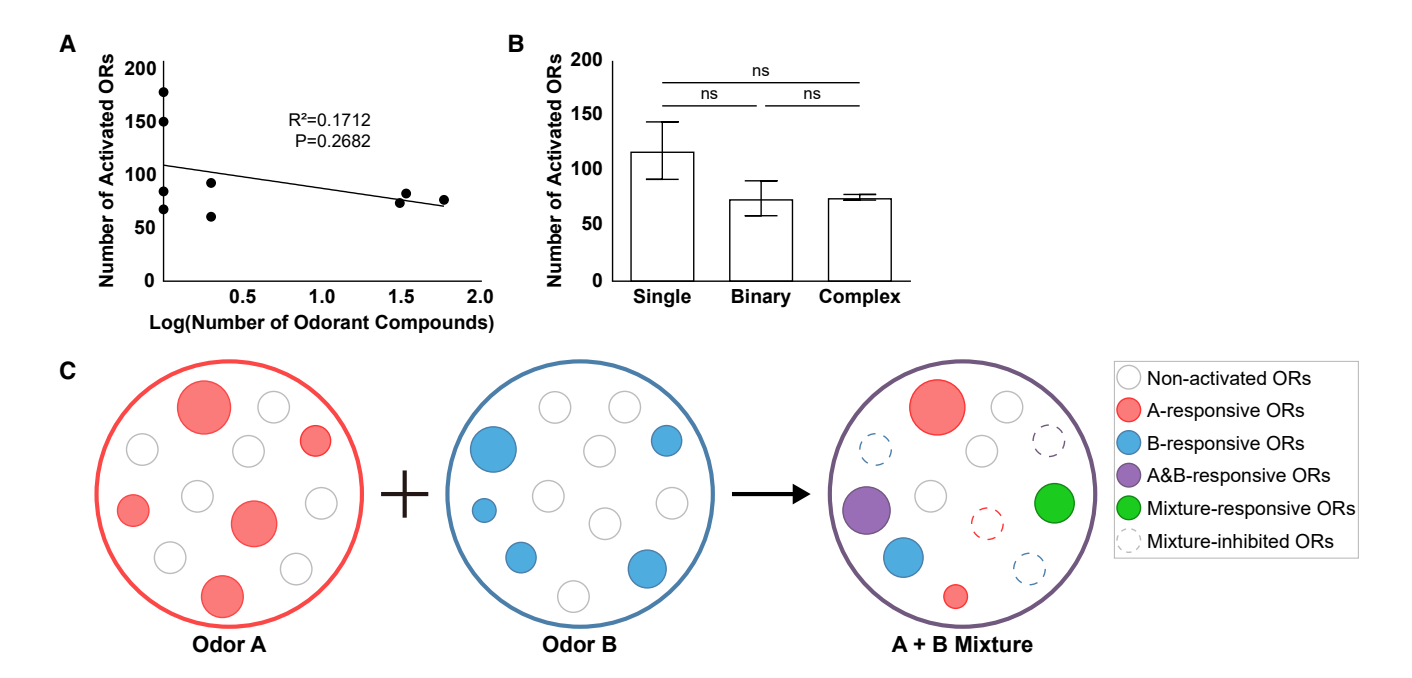


Figure 4. Statistical analysis of the number of activated olfactory receptors in response to odors of varying complexity

(A) Scatterplot depicting the relationship between the number of chemical components in each odor stimulus (x axis) and the corresponding number of activated olfactory receptors (ORs) (y axis). Data include single odorants, binary mixtures, and complex naturalistic fragrances. No significant correlation was observed. (B) Bar graph comparing mean activated OR counts among stimulus complexity categories: single chemical compounds (119.75  $\pm$  26.41, n = 4), binary mixtures (76.0  $\pm$  16.0, n = 2), and complex fragrances (77.0  $\pm$  2.65, n = 3). Data are represented as mean  $\pm$  SEM. One-way ANOVA indicates no significant differences among groups (p = 0.3188).

(C) Schematic model illustrating olfactory receptor coding at the receptor level. Individual odor-responsive ORs remain active (overlapping area), some ORs exhibit suppression in mixtures (non-overlapping in single odors), and new mixture-specific ORs emerge. This integrated response maintains stable total OR activation regardless of odor complexity.

certain individual odor-non-responsive ORs are activated. This integration spares the total number of activated ORs while generating distinct activation patterns for different odors.

Mechanistically, these response profiles are consistent with established principles of odor-receptor interactions. Suppression of OR activation in mixtures can be explained by receptor antagonism or competitive binding between odorant molecules at the receptor site, a phenomenon demonstrated in previous studies. For some ORs not responsive to single odorants but to odor mixtures, this emergent activity may result from allosteric modulation, cooperative binding, or non-linear network effects at either the receptor or circuit level. 25

For all analyses, ORs were assigned to each response category based on pre-defined fold-change and p value thresholds. While our study does not directly distinguish the underlying molecular mechanisms for every OR, the observed categories align with known modes of receptor modulation and provide a descriptive framework for future mechanistic work.

#### **DISCUSSION**

## Receptor-level mechanisms underlying olfactory mixture processing

We employed phosphoTRAP technology to systematically examine OR activation patterns across the entire receptor repertoire in response to individual odorants and their mixtures. Our

results demonstrate that odorant mixture processing operates through a combination of linear integration and selective nonlinear interactions at the receptor level.

When assessed using binary classification based on statistical thresholds (fold change  $\geq 2$ , p value  $\leq 0.05$ ), the responses of most ORs to odorant mixtures closely matched the linear sum of responses to individual components. These criteria, selected to maintain continuity with established phosphoTRAP and transcriptomic studies, enabled direct comparison with previous work while providing statistical rigor and reproducibility.

However, a statistically significant subset of ORs displayed non-linear response profiles that could not be predicted from single-component responses. Previous studies using *in vivo* imaging and *in vitro* reporter assays have suggested that ORs can exhibit non-linear responses to odorant mixtures. <sup>16,21</sup> Recent systematic analyses have demonstrated that antagonistic interactions at the receptor level are widespread and can modulate mixture representations. <sup>20,22,23</sup> Our findings extend this understanding by providing a comprehensive receptor-level profile of both linear and non-linear responses across a spectrum of odor complexities, from binary mixtures to naturalistic fragrances containing dozens of compounds.

#### Input normalization as a principle of olfactory coding

Input normalization in sensory systems expands dynamic range, enhances contrast, and improves signal-to-noise ratio, while



response normalization further reduces redundancy, maintains perceptual stability, and enables context-dependent processing.<sup>24</sup> Studies in *Drosophila* have demonstrated that both forms of normalization operate in the olfactory system, suggesting these are general sensory principles.<sup>34</sup>

No significant differences in activated OR counts between single compounds, binary mixtures, and complex fragrances were found despite large differences in chemical complexity. This implies that the olfactory periphery may implement input normalization to stabilize receptor recruitment across varying stimulus conditions, although further research with varying odor concentrations is warranted to validate this hypothesis.

These results align with the findings reported by Zak et al. (2024), suggesting that increasing mixture complexity leads to denser olfactory bulb (OB) activation without altering overall population sparseness.<sup>35</sup> These convergent findings support input normalization as a general computation in the OE that constrains receptor recruitment under complex odor conditions. Whereas Zak et al. focused on the OB dynamics via optical imaging, our complementary receptor-level profiling of the OSN demonstrated that normalization emerged at the first stage of olfactory processing.

By preventing receptor saturation and preserving coding capacity in environments containing hundreds of volatile compounds, input normalization likely enhances odor discrimination in noisy settings and improves detection against background stimuli, as theoretical models predict.<sup>25</sup> Elucidating the molecular mechanisms of this normalization will be essential for a deeper understanding of olfactory coding principles.

## Implications for artificial olfaction and sensory technology

Our findings have important implications for the development of artificial olfactory systems. The observation that biological olfactory systems maintain stable receptor activation regardless of mixture complexity provides a conceptual framework for optimizing electronic nose algorithms and sensor designs. Recent developments in multi-thin film transistor sensor arrays demonstrate that normalization and combinatorial coding strategies can improve selectivity and robustness for complex odor detection. <sup>36</sup>

Furthermore, advances in artificial intelligence have shown that computational normalization through embedding spaces can enable a more linear representation of non-linear olfactory interactions, improving odor prediction for complex molecular blends.<sup>37</sup> However, the precise biological mechanisms underlying these computational achievements remain unclear. Future research integrating receptor-level insights from biological olfaction with advances in artificial intelligence may accelerate the development of next-generation sensory technologies.

#### **Future research directions**

Several important questions merit further investigation. First, detailed sequence alignments and comparative analyses of activated ORs, focusing on the 3D structure of orthosteric binding sites, could elucidate the molecular basis of receptor specificity and ligand promiscuity. Advanced structural bioinformatics approaches can help determine whether specific odorants can realistically bind across broad spectra of receptor sites.

Second, the mechanisms underlying non-linear responses and input normalization require systematic investigation. We identified distinct populations of mixture-responsive ORs, including those showing inhibitory interactions and emergent activation patterns, but the molecular basis underlying these phenomena remains unclear. Understanding whether these effects result from direct receptor-level interactions, allosteric modulation, or network-level computations can help advance olfactory coding theory.

Finally, the generality of input normalization across different stimulus conditions requires validation. We delivered high concentrations over extended periods, which may have influenced the observed patterns. Future studies using behaviorally titrated concentrations and controlled vapor-phase delivery systems should assess whether normalization occurs under more physiological conditions.

In summary, our findings show that olfactory mixture encoding reflects mostly linear integration of component responses combined with a smaller set of non-linear receptor interactions. This hybrid coding strategy maintains stable receptor recruitment as mixture complexity increases, and the minority of non-linear responses adds specificity to enhance mixture discrimination. By preventing receptor saturation and preserving coding capacity, this efficient scheme ensures robust odor detection in natural environments. Our insights pave the way for future studies into the molecular mechanisms of peripheral olfactory processing and their translation into artificial sensory systems.

#### **Limitations of the study**

Our experimental approach of co-applying binary odorants to filter paper does not provide precise control over vapor-phase concentrations or account for potential chemical interactions between the components. The vapor pressure differences among odorants may result in actual airborne ratios that deviate from the intended proportion, potentially influencing OR activation independent of receptor-level mechanisms. Future studies using an olfactometer with vapor-phase mixing capabilities can improve stimulus control and enable more precise investigation of concentration-dependent effects.

All odorants were delivered at high concentrations for extended periods, raising the possibility of ceiling effects or non-specific receptor activation. The use of high concentrations may mask subtle differences in receptor engagement that occur at more physiologically relevant intensities. Evaluating responses across broader concentration ranges, including near-threshold levels, is essential for determining the robustness of observed normalization patterns under natural conditions.

We used freely moving mice during odor exposure, which may have introduced behavioral variability affecting receptor activation. Variations in odor investigation patterns, distance from the odor source, or exploratory locomotion could alter stimulus access and influence OR responses. Using head-fixed preparations with precise vapor-phase delivery can reduce the effects of these confounders.

Future work should expand the scope by testing multiple classes of odorants across graded concentrations and varied mixture ratios. Conducting larger systematic experiments can





provide clearer insights into the contributions of linear and nonlinear integration mechanisms.

While phosphoTRAP enables unbiased, genome-wide profiling of receptor activation, the method inherently links transcript abundance to statistical detection power. In this study, approximately 30% of detected ORs exhibited low read counts (<10), reducing the power to detect differential expression when counts are very low. However, most ORs showing biologically relevant responses possessed sufficient coverage for reliable statistical assessment. Nonetheless, some ORs with substantial fold changes may not have achieved statistical significance solely because of low abundance, reflecting the trade-off between biological and statistical criteria in RNAsequencing analysis. Importantly, rigid fold-change and p value thresholds must be interpreted in the context of coverage, and while they guard against false positives, they can obscure functionally meaningful receptor activation at the margins of detectability.

#### **RESOURCE AVAILABILITY**

#### Lead contact

Requests for further information and resources should be directed to and will be fulfilled by the lead contact, Han Kyoung Choe (choehank@dgist.ac.kr).

#### **Materials availability**

This study did not generate new, unique reagents or materials.

#### Data and code availability

- RNA-sequencing data of total RNA and pS6-IP mRNA have been deposited at GEO: GSE296359, GEO: GSE296360, and GEO: GSE306619.
- This paper does not report original code.
- Any additional information required to reanalyze the data reported in this paper is available from the lead contact upon request.

#### **ACKNOWLEDGMENTS**

This research was supported by Basic Science Research Program through the National Research Foundation of Korea (NRF) funded by the Ministry of Education (RS-2020-NR049577) and by a National Research Foundation of Korea (NRF) grant funded by the Ministry of Science and ICT of the Korean government (RS-2024-00428887). We thank Byungsoo Kang (SYSOFT, Daegu, Republic of Korea) for supporting the RNA sequencing.

#### **AUTHOR CONTRIBUTIONS**

Conceptualization, M.K. and H.K.C.; data curation, M.K.; formal analysis, M.K. and J.L.; funding acquisition, H.-J.K. and C.M.; investigation, M.K.; methodology, M.K., I.P., and J.K.; resources, K.L.; supervision, H.K.C.; visualization, M.K.; writing - original draft, M.K.; writing - review & editing, M.K., K.L., J.S., J.-W.C., J.E.J., H.-J.K., C.M., and H.K.C.

#### **DECLARATION OF INTERESTS**

The authors declare no competing interests.

#### **DECLARATION OF GENERATIVE AI AND AI-ASSISTED TECHNOLOGIES IN THE WRITING PROCESS**

During the preparation of this work, the authors used Google Gemini in order to compose English sentences that clearly convey meaning. After using this tool or service, the authors reviewed and edited the content as needed and take full responsibility for the content of the publication.

#### **STAR**\*METHODS

Detailed methods are provided in the online version of this paper and include the following:

- KEY RESOURCES TABLE
- EXPERIMENTAL MODEL AND STUDY PARTICIPANT DETAILS
- Animals
- METHOD DETAILS
  - Odor stimulation
  - o Immunohistochemistry
  - Odor preference test
  - o Homogenization of olfactory epithelium tissues
  - O Western blot analysis
  - o Preparation of magnetic beads
  - o RNA isolation and ribosome immunoprecipitation
- QUANTIFICATION AND STATISTICAL ANALYSIS
  - o RNA quality assessment and sequencing
  - RNA-seq data analysis
  - O Differential gene expression analysis
  - o Principal component analysis (PCA)
  - Heatmap analysis
  - o Full OR activation space analysis
  - o Correlation analysis
  - o Venn diagram analysis

#### SUPPLEMENTAL INFORMATION

Supplemental information can be found online at https://doi.org/10.1016/j.isci. 2025.113740.

Received: May 12, 2025 Revised: September 8, 2025 Accepted: October 7, 2025 Published: October 10, 2025

#### REFERENCES

- 1. Firestein, S. (2001). How the olfactory system makes sense of scents. Nature 413, 211-218, https://doi.org/10.1038/35093026.
- 2. Ache, B.W., and Young, J.M. (2005). Olfaction: Diverse Species, Conserved Principles. Neuron 48, 417-430. https://doi.org/10.1016/j. neuron.2005.10.022.
- 3. Buck, L., and Axel, R. (1991). A novel multigene family may encode odorant receptors: a molecular basis for odor recognition. Cell 65, 175-187. https://doi.org/10.1016/0092-8674(91)90418-x.
- 4. Zhang, X., and Firestein, S. (2002). The olfactory receptor gene superfamily of the mouse. Nat. Neurosci. 5, 124-133. https://doi.org/10.1038/
- 5. Malnic, B., Hirono, J., Sato, T., and Buck, L.B. (1999). Combinatorial receptor codes for odors. Cell 96, 713-723. https://doi.org/10.1016/ s0092-8674(00)80581-4.
- 6. Bushdid, C., Magnasco, M.O., Vosshall, L.B., and Keller, A. (2014). Humans can discriminate more than 1 trillion olfactory stimuli. Science 343, 1370-1372. https://doi.org/10.1126/science.1249168.
- 7. del Mármol, J., Yedlin, M.A., and Ruta, V. (2021). The structural basis of odorant recognition in insect olfactory receptors. Nature 597, 126-131. https://doi.org/10.1038/s41586-021-03794-8.
- 8. Billesbølle, C.B., de March, C.A., van der Velden, W.J.C., Ma, N., Tewari, J., del Torrent, C.L., Li, L., Faust, B., Vaidehi, N., Matsunami, H., et al. (2023). Structural basis of odorant recognition by a human odorant receptor. Nature 615, 742-749. https://doi.org/10.1038/s41586-023-05798-y.
- 9. Choi, C., Bae, J., Kim, S., Lee, S., Kang, H., Kim, J., Bang, I., Kim, K., Huh, W.-K., Seok, C., et al. (2023). Understanding the molecular mechanisms of



- odorant binding and activation of the human OR52 family. Nat. Commun. *14*. 8105. https://doi.org/10.1038/s41467-023-43983-9.
- Zhao, J., Chen, A.Q., Ryu, J., and del Mármol, J. (2024). Structural basis of odor sensing by insect heteromeric odorant receptors. Science 384, 1460–1467. https://doi.org/10.1126/science.adn6384.
- Wang, J., Zhang, Q., Fan, W., Shi, Q., Mao, J., Xie, J., Chai, G., and Zhang, C. (2024). Deciphering olfactory receptor binding mechanisms: a structural and dynamic perspective on olfactory receptors. Front. Mol. Biosci. 11, 1498796. https://doi.org/10.3389/fmolb.2024.1498796.
- Ressler, K.J., Sullivan, S.L., and Buck, L.B. (1993). A zonal organization of odorant receptor gene expression in the olfactory epithelium. Cell 73, 597–609. https://doi.org/10.1016/0092-8674(93)90145-G.
- Nara, K., Saraiva, L.R., Ye, X., and Buck, L.B. (2011). A Large-Scale Analysis of Odor Coding in the Olfactory Epithelium. J. Neurosci. 31, 9179–9191. https://doi.org/10.1523/JNEUROSCI.1282-11.2011.
- Jiang, Y., Gong, N.N., Hu, X.S., Ni, M.J., Pasi, R., and Matsunami, H. (2015). Molecular profiling of activated olfactory neurons identifies odorant receptors for odors *in vivo*. Nat. Neurosci. 18, 1446–1454. https://doi.org/ 10.1038/nn.4104.
- Singh, V., Murphy, N.R., Balasubramanian, V., and Mainland, J.D. (2019). Competitive binding predicts nonlinear responses of olfactory receptors to complex mixtures. Proc. Natl. Acad. Sci. USA 116, 9598–9603. https://doi. org/10.1073/pnas.1813230116.
- de March, C.A., Titlow, W.B., Sengoku, T., Breheny, P., Matsunami, H., and McClintock, T.S. (2020). Modulation of the combinatorial code of odorant receptor response patterns in odorant mixtures. Mol. Cell. Neurosci. 104, 103469. https://doi.org/10.1016/j.mcn.2020.103469.
- Krishnamurthy, K., Hermundstad, A.M., Mora, T., Walczak, A.M., and Balasubramanian, V. (2022). Disorder and the Neural Representation of Complex Odors. Front. Comput. Neurosci. 16, 917786. https://doi.org/10.3389/fncom.2022.917786.
- Thomas-Danguin, T., Sinding, C., Romagny, S., El Mountassir, F., Atanasova, B., Le Berre, E., Le Bon, A.-M., and Coureaud, G. (2014). The perception of odor objects in everyday life: a review on the processing of odor mixtures. Front. Psychol. 5, 504. https://doi.org/10.3389/fpsyg. 2014.00504.
- Rokni, D., Hemmelder, V., Kapoor, V., and Murthy, V.N. (2014). An olfactory cocktail party: figure-ground segregation of odorants in rodents. Nat. Neurosci. 17, 1225–1232. https://doi.org/10.1038/nn.3775.
- Xu, L., Li, W., Voleti, V., Zou, D.-J., Hillman, E.M.C., and Firestein, S. (2020). Widespread receptor-driven modulation in peripheral olfactory coding. Science 368, eaaz5390. https://doi.org/10.1126/science.aaz5390.
- Pfister, P., Smith, B.C., Evans, B.J., Brann, J.H., Trimmer, C., Sheikh, M., Arroyave, R., Reddy, G., Jeong, H.-Y., Raps, D.A., et al. (2020). Odorant Receptor Inhibition Is Fundamental to Odor Encoding. Curr. Biol. 30, 2574–2587.e6. https://doi.org/10.1016/j.cub.2020.04.086.
- Zak, J.D., Reddy, G., Vergassola, M., and Murthy, V.N. (2020). Antagonistic odor interactions in olfactory sensory neurons are widespread in freely breathing mice. Nat. Commun. 11, 3350. https://doi.org/10.1038/s41467-020-17124-5.
- Trimmer, C., Arroyave, R., Vuilleumier, C., Wu, L., Dumer, A., DeLaura, C., Kim, J., Pierce, G.M., Borisovska, M., De Nanteuil, F., et al. (2023). Allosteric modulation of a human odorant receptor. Curr. Biol. 33, 1523– 1534.e4. https://doi.org/10.1016/j.cub.2023.03.016.
- Carandini, M., and Heeger, D.J. (2011). Normalization as a canonical neural computation. Nat. Rev. Neurosci. 13, 51–62. https://doi.org/10.1038/nrn3136.
- Reddy, G., Zak, J.D., Vergassola, M., and Murthy, V.N. (2018). Antagonism in olfactory receptor neurons and its implications for the perception of odor mixtures. eLife 7, e34958. https://doi.org/10.7554/eLife.34958.

- Belluscio, L., Gold, G.H., Nemes, A., and Axel, R. (1998). Mice Deficient in Golf Are Anosmic. Neuron 20, 69–81. https://doi.org/10.1016/S0896-6273 (00)80435-3.
- Wong, S.T., Trinh, K., Hacker, B., Chan, G.C., Lowe, G., Gaggar, A., Xia, Z., Gold, G.H., and Storm, D.R. (2000). Disruption of the Type III Adenylyl Cyclase Gene Leads to Peripheral and Behavioral Anosmia in Transgenic Mice. Neuron 27, 487–497. https://doi.org/10.1016/S0896-6273(00) 00060-X.
- Ibarra-Soria, X., Nakahara, T.S., Lilue, J., Jiang, Y., Trimmer, C., Souza, M.A., Netto, P.H., Ikegami, K., Murphy, N.R., Kusma, M., et al. (2017).
   Variation in olfactory neuron repertoires is genetically controlled and environmentally modulated. eLife 6, e21476. https://doi.org/10.7554/eLife.21476.
- Nakashima, A., Sato, T., and Tamanoi, F. (2010). Fission yeast TORC1 regulates phosphorylation of ribosomal S6 proteins in response to nutrients and its activity is inhibited by rapamycin. J. Cell Sci. 123, 777–786. https://doi.org/10.1242/jcs.060319.
- Meyuhas, O. (2008). Chapter 1 Physiological Roles of Ribosomal Protein S6: One of Its Kind. Int Rev Cell Mol Biol. 268, 1–37. https://doi.org/10. 1016/S1937-6448(08)00801-0.
- Biever, A., Valjent, E., and Puighermanal, E. (2015). Ribosomal Protein S6 Phosphorylation in the Nervous System: From Regulation to Function. Front. Mol. Neurosci. 8, 75. https://doi.org/10.3389/fnmol.2015.00075.
- Knight, Z.A., Tan, K., Birsoy, K., Schmidt, S., Garrison, J.L., Wysocki, R. W., Emiliano, A., Ekstrand, M.I., and Friedman, J.M. (2012). Molecular Profiling of Activated Neurons by Phosphorylated Ribosome Capture. Cell 151, 1126–1137. https://doi.org/10.1016/j.cell.2012.10.039.
- Serizawa, S., Miyamichi, K., and Sakano, H. (2004). One neuron-one receptor rule in the mouse olfactory system. Trends Genet. 20, 648–653. https://doi.org/10.1016/j.tig.2004.09.006.
- Olsen, S.R., Bhandawat, V., and Wilson, R.I. (2010). Divisive Normalization in Olfactory Population Codes. Neuron 66, 287–299. https://doi.org/10. 1016/j.neuron.2010.04.009.
- Zak, J.D., Reddy, G., Konanur, V., and Murthy, V.N. (2024). Distinct information conveyed to the olfactory bulb by feedforward input from the nose and feedback from the cortex. Nat. Commun. 15, 3268. https://doi.org/10.1038/s41467-024-47366-6.
- Kim, S., Pyo, G., Choi, W., Jang, H.W., Kwon, H., Kim, K., Heo, S.J., Kim, D.S., Kim, J., Lee, Y., et al. (2025). Electronic Nose Based on a Multi-Thin Film Transistor Sensor Array Structure for Detecting Odorants with High Selectivity. Anal. Sens. 2500003. https://doi.org/10.1002/anse. 202500003.
- Sisson, L., Barsainyan, A.A., Sharma, M., and Kumar, R. (2025). Deep Learning for Odor Prediction on Aroma-Chemical Blends. ACS Omega 10, 8980–8992. https://doi.org/10.1021/acsomega.4c07078.
- Cometto-Muñiz, J.E., Cain, W.S., and Abraham, M.H. (2003). Quantification of Chemical Vapors in Chemosensory Research. Chem. Senses 28, 467–477. https://doi.org/10.1093/chemse/28.6.467.
- Dobin, A., Davis, C.A., Schlesinger, F., Drenkow, J., Zaleski, C., Jha, S., Batut, P., Chaisson, M., and Gingeras, T.R. (2013). STAR: ultrafast universal RNA-seq aligner. Bioinformatics 29, 15–21. https://doi.org/10.1093/bioinformatics/bts635.
- Patro, R., Duggal, G., Love, M.I., Irizarry, R.A., and Kingsford, C. (2017).
   Salmon provides fast and bias-aware quantification of transcript expression. Nat. Methods 14, 417–419. https://doi.org/10.1038/nmeth.4197.
- Zhu, A., Ibrahim, J.G., and Love, M.I. (2019). Heavy-tailed prior distributions for sequence count data: removing the noise and preserving large differences. Bioinformatics 35, 2084–2092. https://doi.org/10.1093/bioinformatics/bty895.
- Pantano, L. (2024). DEGreport: Report of DEG analysis. http://lpantano. github.io/DEGreport/.





- 43. Love, M.I., Huber, W., and Anders, S. (2014). Moderated estimation of fold change and dispersion for RNA-seq data with DESeq2. Genome Biol. *15*, 550. https://doi.org/10.1186/s13059-014-0550-8.
- 44. Blighe, K., Rana, S., and Lewis, M. (2024). EnhancedVolcano: Publication-ready volcano plots with enhanced colouring and labeling. https://github.com/kevinblighe/EnhancedVolcano.
- 45. Wickham, H. (2016). Data Analysis. In ggplot2. Use R! (Cham: Springer), pp. 189–201. https://doi.org/10.1007/978-3-319-24277-4\_9.
- Kolde, R. (2019). Package name: pheatmap: Pretty Heatmaps. https:// CRAN.R-project.org/package=pheatmap.
- Neuwirth, E. (2022). RColorBrewer: ColorBrewer Palettes. https://CRAN. R-project.org/package=RColorBrewer.
- 48. Huber, W., and Reyes, A. (2025). pasilla: Data package with per-exon and per-gene read counts of RNA-seq samples of Pasilla knock-down by Brooks et al. Genome Res. 2011. https://bioconductor.org/packages/pasilla/.
- Wickham, H., Averick, M., Bryan, J., Chang, W., McGowan, L., François, R., Grolemund, G., Hayes, A., Henry, L., Hester, J., et al. (2019). Welcome to the Tidyverse. J. Open Source Softw. 4, 1686. https://doi.org/10.21105/ joss.01686.



#### **STAR**\*METHODS

#### **KEY RESOURCES TABLE**

REAGENT or RESOURCE	SOURCE	IDENTIFIER
Antibodies		
Rabbit polyclonal anti-phospho S6 (Ser244, Ser247)	Thermo Fisher Scientific	Cat# 44-923G; RRID: AB_2533798
Goat polyclonal anti-olfactory marker protein	FUJIFILM Wako Pure Chemical Corporation	Cat# 019-22291; RRID: AB_3094987
Cy3-conjugated donkey anti-rabbit IgG	Jackson ImmunoResearch Labs	Cat# 711-165-152; RRID: AB_2307443
Alexa Fluor 488-conjugated donkey anti-goat gG	Jackson ImmunoResearch Labs	Cat# 705-545-003; RRID: AB_2340428
Normal Donkey Serum	Jackson ImmunoResearch Labs	Cat# 017-000-121; RRID: AB_2337258
HRP-conjugated β-Actin Antibody (C4)	Santa Cruz Biotechnology	Cat# sc-47778 HRP; RRID: AB_2714189
Goat anti-Rabbit IgG-heavy and light chain Antibody HRP Conjugated	Bethyl	Cat# A120-101P; RRID: AB_67264
Chemicals, peptides, and recombinant proteins		
Acetophenone	Merck	Cas 98-86-2; Cat# 42163
Cis-3-hexenol	Merck	Cas 928-96-1; Cat# 91316
Decanal	Merck	Cas 112-31-2; Cat# 59581
Octanal	Merck	Cas 124-13-0; Cat# 52466
Floral fragrance	SCENTON INC.	N/A
Mint fragrance	SCENTON INC.	N/A
Floral + Mint fragrance	SCENTON INC.	N/A
Sodium fluoride, 99.99% (metals basis)	Alfa Aesar	Cas 7681-49-4; Cat# 011003
Calyculin A	Cell Signaling Technology	Cas 101932-71-2; Cat# 9902
Bovine Serum Albumin (IgG-Free, Protease- Free)	Jackson Immunoresearch	Cat# 001-000-162; RRID: AB_2336946
cOmplete <sup>TM</sup> , Mini, EDTA-free Protease nhibitor Cocktail	Merck	Cat# 04693159001
2-Mercaptoethanol (β-ME)	Merck	Cas 60-24-2; Cat# 63689
Sodium pyrophosphate dibasic	Merck	Cas 7758-16-9; Cat# 71501
3-Glycerophosphate disodium salt hydrate	Merck	Cas 154804-51-0; Cat# G9422
Sodium orthovanadate	Merck	Cas 13721-39-6; Cat# S6508
RNasin® Ribonuclease Inhibitor	Promega	Cat# N2511
NP-40 Surfact-Amps <sup>TM</sup> Detergent Solution	Thermo Fisher Scientific	Cat# 28324
HEPES (1 M)	Thermo Fisher Scientific	Cat# 15630080
Cycloheximide, 95%	Thermo Fisher Scientific	Cat# 357420010
Dynabeads <sup>TM</sup> Protein A for mmunoprecipitation	Thermo Fisher Scientific	Cat# 10002D
PBS, pH 7.4	Thermo Fisher Scientific	Cat# 10010023
MgCl2 (1 M)	Thermo Fisher Scientific	Cat# AM9530G
CI (2 M), RNase-free	Thermo Fisher Scientific	Cat# AM9640G
Nuclease-Free Water (not DEPC-Treated)	Thermo Fisher Scientific	Cat# AM9932
OTT (dithiothreitol)	Thermo Fisher Scientific	Cat# R0861
Friton X-100	Merck	Cat# X100
Tween 20	VWR	Cat# 0777-1L
Sodium Dodecyl Sulfate (SDS)	Merck	Cat# L5750
Fris ultrapure	Duchefa	Cat# T1501
Glycine	Duchefa	Cat# G0709

(Continued on next page)





Continued		
REAGENT or RESOURCE	SOURCE	IDENTIFIER
Sodium chloride	Duchefa	Cat# S0520
Albumin bovine, fraction V, ≥98%	MPbio	Cat# 160069
NuPAGE LDS Sample Buffer (4X)	Thermo Fisher Scientific	Cat# NP0007
Q-PAGE TGN Precast Gel (Mini, 15 wells, 10%)	SMOBIO Technology	Cat# QP4220
Restore Western Blot Stripping Buffer	Thermo Fisher Scientific	Cat# 21059
Critical commercial assays		
DNF-472 HS RNA (15 nt) Kit	Agilent	Cat# DNF-472-0500
RNase-Free DNase Set	Qiagen	Cat# 79254
RNeasy Mini Kit	Qiagen	Cat# 74104
Pierce BCA Protein Assay Kits	Thermo Fisher Scientific	Cat# 23227
ECL Select Western Blotting Detection Reagent	Cytiva	Cat# RPN2235
Deposited data		
RNA sequencing data files	This paper	GEO: GSE296359, GEO: GSE296360, and GEO: GSE306619
Experimental models: Organisms/strains		
C57BL/6J	The Jackson Laboratory	RRID: IMSR_JAX:000664
Software and algorithms		
Python (version 3.12.3)	Python	https://www.python.org/
STAR (version 2.7.10b)	Dobin et al. <sup>39</sup>	https://github.com/alexdobin/STAR
Salmon (version 1.10.1)	Patro et al. <sup>40</sup>	https://combine-lab.github.io/salmon/
R (version 4.4.2)	The R Project for Statistical Computing	https://www.r-project.org/
apeglm (version 1.26.0)	Zhu et al. <sup>41</sup>	https://bioconductor.org/packages/apeglm/
DEGreport (version 1.40.0)	Pantano. L <sup>42</sup>	https://bioconductor.org/packages/ DEGreport/
DESeq2 (version 1.44.0)	Love et al. <sup>43</sup>	https://bioconductor.org/packages/DESeq2/
EnhancedVolcano (version 1.22.0)	Blighe et al. <sup>44</sup>	https://bioconductor.org/packages/ EnhancedVolcano/
ggplot2 (version 3.5.1)	Wickham. H <sup>45</sup>	https://ggplot2.tidyverse.org/
pheatmap (version 1.0.12)	Kolde. R <sup>46</sup>	https://cran.r-project.org/web/packages/ pheatmap/index.html
RColorBrewer (version 1.1.3)	Erich Neuwirth <sup>47</sup>	https://cran.r-project.org/web/packages/ RColorBrewer/index.html
pasilla (version 1.34.0)	Wolfgang Huber, Alejandro Reyes <sup>48</sup>	https://bioconductor.org/packages/pasilla
Tidyverse	Wickham et al. <sup>49</sup>	https://www.tidyverse.org/packages/
EthoVision XT (version 17.5.1718)	Noldus	https://noldus.com/ethovision-xt
ImageJ	National Institutes of Health	https://imagej.net/ij/index.html
Prism 10	GraphPad	https://www.graphpad.com/

#### **EXPERIMENTAL MODEL AND STUDY PARTICIPANT DETAILS**

#### **Animals**

C57BL/6J wildtype male mice (RRID: IMSR\_JAX:000664) were housed in the Specific Pathogen Free (SPF) area of the Laboratory Animal Resource Center at Daegu Gyeongbuk Institute of Science and Technology (DGIST). The mice were maintained under a 12-h light/dark cycle with ad libitum access to standard rodent chow and water. To ensure a clean environment, cages were replaced regularly. All experimental procedures were approved by the Institutional Animal Care and Use Committee of DGIST (Approval number: DGIST-IACUC-25040908-0001) and were conducted in accordance with the guidelines for the care and use of laboratory animals.



#### **METHOD DETAILS**

#### **Odor stimulation**

C57BL/6J wildtype male mice (8 weeks old) were individually placed into sealed containers ( $403 \times 165 \times 175$  mm, W  $\times$  D  $\times$  H; volume  $\approx 11.6$  L) within an experimental animal housing facility. The facility was equipped with independent ventilation systems for each room to prevent odorant mixing. Mice were habituated for 4 h in an odorless environment before exposure. For single odorant conditions, 10  $\mu$ L of undiluted (100%) acetophenone, decanal, octanal, or *cis*-3-hexenol (Merck) was applied directly onto a 1 cm  $\times$  1 cm filter paper placed in a 35 mm culture dish. For binary mixture conditions, 10  $\mu$ L of each undiluted (100%) component was applied separately but simultaneously to the same filter paper (total 20  $\mu$ L per dish), ensuring the absolute amount of each odorant in the mixture matched that of its corresponding single odorant condition. For complex fragrances (floral, mint, and floral—mint blend; SCENTON INC.), 10  $\mu$ L of undiluted product was applied per dish. A filter paper with no odorant served as the control. The prepared dish was then placed into the mouse container, and the mouse was exposed for 90 min. Each condition and control was tested with three mice (n = 3), using littermates of the same sex to minimize biological variability.

#### **Immunohistochemistry**

After odor stimulation, mice were transcardially perfused first with PBS to remove blood, followed by 4% paraformaldehyde (PFA) to fix tissues. The olfactory epithelium (OE) was dissected and post-fixed overnight in 4% PFA at 4°C. For cryoprotection, tissues were incubated in 30% sucrose solution overnight at 4°C. Cryoprotected samples were embedded in OCT compound and frozen at -80°C. The OE was cryosectioned at -25°C into  $50~\mu m$  slices. Sections were mounted onto glass slides and air-dried at 37°C for at least 30min.

To remove residual OCT, slides were washed in PBS three times for 5min each on a shaker at 30 RPM. Tissue sections were blocked for 2h at room temperature with 5% normal donkey serum in 0.1% PBST (PBS with 0.1% Triton X-100). Sections were then incubated overnight at 4°C with primary antibodies diluted 1:1,000 in 0.1% PBST: rabbit anti-phospho-S6 (Ser244, Ser247) and goat anti-OMP. After primary incubation, slides were washed six times for 5min each in 0.1% PBST on a shaker at 30 RPM. Secondary antibody incubation was performed at room temperature for 2h using donkey anti-rabbit Cy3 and donkey anti-goat Alexa Fluor 488, both at 1:1,000 dilution in 0.1% PBST. After incubation with secondary antibodies, slides were again washed three times for 5min each in 0.1% PBST on a shaker at 30 RPM. Sections were mounted with mounting solution and placed on a coverslip. Stained OE samples were imaged using confocal microscopy at 20x magnification.

#### **Odor preference test**

C57BL/6J wild-type male mice (8 weeks old) were individually housed in new sealed containers ( $403 \times 165 \times 175$  mm, W × D × H; volume  $\approx 11.6$  L) for habituation one day prior to the experiment. On the test day, each mouse was exposed alternately to a no-odor filter paper and a filter paper soaked with an odor solution, each for 5 min, in cages with the lids removed. Filter papers (1 cm × 1 cm) were placed in 35 mm dishes for odor presentation. Each experimental session included exposure to three different odors per day, and over a total of three days, each animal was exposed to all nine odors (n = 7). The order of odor presentation was randomized to avoid sequence-dependent preferences. Mouse behavior was recorded using a camera positioned above the cage, and all behavioral videos were analyzed with EthoVision XT software.

#### Homogenization of olfactory epithelium tissues

The C57BL/6J wildtype male mice (8 weeks old) were euthanized by cervical dislocation following odorant stimulation. Immediately after euthanasia, perfusion was performed using chilled perfusion buffer (PBS, 5 mM NaF, 2.5 mM Na $_3$ VO $_4$ , 2.5 mM Na $_4$ P $_2$ O $_7$ , 5 mM  $_5$ -glycerophosphate, 100  $_{\rm H}$ g/mL cycloheximide, and one tablet of Roche cOmplete protease inhibitor per 100 mL). A total of 10 mL of perfusion buffer was used to remove blood from the olfactory epithelium (OE) tissue. The OE was immediately sampled and placed into a 2 mL tube containing 1.5 mL of homogenization buffer (10 mM HEPES [pH 7.4], 150 mM KCl, 10 mM MgCl $_2$ , 100 mM calyculin A, 0.5 mM DTT, 100 U/mL RNasin (Promega), 250  $_{\rm H}$ g/mL cycloheximide, and one tablet of Roche cOmplete protease inhibitor per 50 mL) on ice. The OE tissue was homogenized using a TissueLyser II (Qiagen) for 2 min at a frequency of 20 Hz in the homogenization buffer. The tissue homogenates were centrifuged at 2,000  $_{\rm X}$  g for 10 min at 4°C. The supernatant was transferred to a new tube, and 105  $_{\rm H}$ L of 10% NP-40 was added to the solution. After gently mixing by inversion and incubating on ice for 2 min, the mixture was centrifuged at 20,000  $_{\rm X}$  g for 10 min at 4°C. The supernatant was used for western blot or immunoprecipitation analyses.

#### Western blot analysis

Protein concentrations of olfactory epithelium (OE) homogenates were measured using the BCA assay. Samples were adjusted to equal protein concentrations and denatured by incubation with NuPAGE LDS sample buffer at 95°C for 5min, then rapidly cooled on ice. Equal amounts of protein were loaded onto 10% polyacrylamide gels and subjected to SDS-PAGE (100V, 100min). Proteins were transferred onto PVDF membranes (0.2A, 90 min). All subsequent membrane processing steps were carried out on a shaker at 30 RPM.





Membranes were blocked with 5% bovine serum albumin (BSA) in 0.2% TBST for 1h at room temperature. Detection of pS6 and  $\beta$ -actin was performed sequentially on the same membrane to ensure antibody specificity. For pS6 detection, membranes were incubated with primary antibody (1:1,000 in 0.2% TBST) for 2h at room temperature, followed by eight washes (5min each) in 0.2% TBST. Membranes were then incubated with anti-rabbit HRP-conjugated secondary antibody (1:20,000 in 0.2% TBST) for 40min at room temperature and washed three times for 5min each.

Protein bands were visualized using enhanced chemiluminescence (ECL) and detected using a Bio-Rad ChemiDoc system. Following detection of the pS6 signal, membranes were stripped using an antibody stripping buffer at room temperature for 30min and washed with 0.2% TBST. Membranes were then re-blocked with 5% BSA in 0.2% TBST for 1 h at room temperature. For  $\beta$ -actin detection, membranes were incubated with HRP-conjugated  $\beta$ -actin antibody (1:20,000 in 0.2% TBST) for 40 min at room temperature and washed three times for 5 min each in 0.2% TBST. Detection was performed using ECL, as above. Band intensities were quantified using ImageJ software.

#### **Preparation of magnetic beads**

A 200  $\mu$ L of Protein A Dynabeads (Invitrogen) was washed twice with Wash Buffer A (10 mM HEPES [pH 7.4], 10 mM MgCl<sub>2</sub>, 150 mM KCl, 1% NP-40) using a magnetic rack to remove the supernatant. The washed beads were then resuspended in Pre-coupling Buffer (10 mM HEPES [pH 7.4], 10 mM MgCl<sub>2</sub>, 150 mM KCl, 1% NP-40, 2% IgG-free BSA), and mixed with 6  $\mu$ L of pS6 antibody (Invitrogen #44-923G). The mixture was incubated at 4°C overnight with rotation to allow for antibody coupling. Following overnight incubation, the beads were washed twice with Wash Buffer A to remove unbound antibody. The beads were then resuspended in 400  $\mu$ L of homogenization buffer and added with 28  $\mu$ L of 10% NP-40. The beads were kept on ice until the immunoprecipitation steps were initiated.

#### RNA isolation and ribosome immunoprecipitation

The following protocol for ribosome immunoprecipitation was adapted from previous works with modifications.  $^{14,32}$  For total RNA isolation, a 50  $\mu$ L aliquot of the OE homogenate was transferred to a new 1.5 mL tube. 350  $\mu$ L of Buffer RLT (included in the RNeasy Mini Kit, QIAGEN) was added to the sample on ice and incubated for 5 min. The RNA was then purified using the RNeasy Mini Kit (QIAGEN) according to the manufacturer's protocol, including an on-column DNase digestion step using the RNase-Free DNase Set (QIAGEN) to eliminate genomic DNA contamination.

For ribosome immunoprecipitation, the prepared pS6 antibody-coupled Protein A Dynabeads were mixed with the remaining OE homogenate and incubated for 1 h at room temperature with gentle rotation. Following incubation, the beads were washed four times with Wash Buffer B (10 mM HEPES [pH 7.4], 350 mM KCl, 5 mM MgCl<sub>2</sub>, 2 mM DTT, 1% NP-40, 100 U/mL RNasin, and 100  $\mu$ g/mL cycloheximide). During the third wash, the beads were transferred to a new tube and incubated at room temperature for 10 min. After the final wash, mRNA was eluted by adding 350  $\mu$ L of Buffer RLT to the beads and incubating for 5 min on ice. The beads were removed using a magnetic rack, and the mRNA was purified using the RNeasy Mini Kit (QIAGEN) following the manufacturer's instructions, including the on-column DNase digestion step.

#### **QUANTIFICATION AND STATISTICAL ANALYSIS**

#### RNA quality assessment and sequencing

The quality and quantity of both total RNA and mRNA were assessed using an Agilent 5200 Fragment Analyzer with the Agilent DNF-472 (15 nt) HS RNA Kit. Libraries were prepared using the TruSeq Stranded mRNA Sample Prep kit (Illumina), and sequencing was carried out on an Illumina NovaSeq 6000 platform according to the manufacturer's protocols. RNA sequencing and genome alignment were performed by SYSOFT (Daegu, Republic of Korea) as a commercial service. Raw reads can be accessed at GEO: GSE296359, GEO: GSE296360, and GEO: GSE306619.

#### RNA-seq data analysis

RNA-seq data analysis was performed using integrated Python and R programming environments. Raw read counts were generated through a pipeline involving read mapping with the STAR aligner and transcript quantification using Salmon, yielding gene-level count data for analysis.<sup>40</sup>

#### Differential gene expression analysis

Differential gene expression analysis was conducted using the DESeq2 R package. To address multiple hypothesis testing, p-values were adjusted using the Benjamini-Hochberg false discovery rate (FDR) method, controlling the expected proportion of false positives. Genes with a p-value  $\leq 0.05$  and an absolute  $\log_2$  fold change ( $\log_2$ FC)  $\geq 1$  were considered significantly differentially expressed. The  $\log_2$ FC estimates were further improved by reducing estimation bias and variance using Bayesian shrinkage as implemented in the apeglm package. This approach uses an approximate posterior estimation for generalized linear model (GLM) coefficients, providing more stable and accurate effect size estimates, particularly for genes with low counts or high variability.





For exploratory data analysis, variance-stabilizing transformation (vst) was applied to normalized counts for calculating sample-to-sample distance matrices based on Euclidean distances. These distances were visualized as heatmaps to assess sample relatedness.

#### Principal component analysis (PCA)

Principal component analysis (PCA) was performed on vst-transformed counts to summarize global expression patterns. PCA visualization incorporated group-specific color schemes, along with plotting of group centroids and vectors to illustrate additive or interactive effects among experimental conditions.

Volcano plots illustrating differential expression results were generated using raw *p*-values and log2FC.<sup>44</sup> Genes exceeding predefined fold change and *p*-value thresholds were highlighted to facilitate candidate gene identification.

#### **Heatmap analysis**

Significantly differentially expressed genes were additionally visualized using heatmaps based on regularized log-transformed (rlog) counts. Gene expression was normalized relative to control group means, and hierarchical clustering was applied to genes while preserving sample order to maintain experimental design context. 46

To visualize and compare OR activation patterns across samples, z-scores were calculated for each OR gene. Specifically, for each gene, the mean and standard deviation of expression values were computed across the biological replicates within each experimental condition (n = 3). Individual expression values were then transformed by subtracting the group mean and dividing by the group standard deviation. These z-scores were used solely for data visualization and exploratory analyses and not as criteria for statistical significance.

#### Full OR activation space analysis

Full OR activation space analysis was performed to evaluate relationships in OR activation patterns across experimental conditions. For each binary odor mixture, the average log2FC from the two individual odor conditions was compared with the log2FC observed in the mixture condition. Pairs of valid values were assessed by Pearson's correlation (R and p-value) and linear regression ( $R^2$ ), and scatterplots with fitted regression lines were generated to illustrate concordance.

#### **Correlation analysis**

Correlations between mixture ("+") and separated ("&") groups were assessed to evaluate the effect of odor presentation format on OR expression patterns. For each odor pair, log2FC estimates for OR genes from the mixture ("+") presentation were compared with those from the separated ("&") presentation. Pairs of valid log2FC values were evaluated by Pearson's correlation (R and p-value) and linear regression (R<sup>2</sup>), and scatterplots with fitted regression lines were generated to illustrate the impact of presentation format on OR activation patterns.

#### Venn diagram analysis

Overlap of significant gene sets across conditions was assessed via Venn diagrams generated using Python's matplotlib\_venn package, employing significance criteria consistent with those used in differential expression analyses.

All statistical testing and thresholds were applied uniformly across analyses to ensure reproducibility and transparency of findings.